

# The Fermionic Axion Interferometer

Nicolò Crescini\*

Fondazione Bruno Kessler (FBK), I-38123, Trento, Italy and  
Univ. Grenoble Alpes, CNRS, Grenoble INP, Institut Néel, 38000 Grenoble, France

The axion is an hypothetical beyond the Standard Model particle. Its experimental search is an ongoing effort, and an expanding number of techniques keep on narrowing its parameters space. Leveraging the interaction between dark matter axions and spins, a fermionic interferometer is an experiment which aims at detecting the axion-induced precession of a spin resonance. We describe the detection scheme, outline the possible experimental implementations, their sensitive axion-mass range and discovery potential. Furthermore, the building and characterisation of an axion interferometer is explained in details and the resulting setup is used to search for sub-neV dark matter.

## Axions and spins

The main evidences of physics beyond the Standard Model [1] are the strong CP problem, the asymmetry between matter and anti-matter, neutrino oscillations, dark matter and dark energy [2]. The axion [3] is an hypothetical particle which has the potential to solve two of these matters. Originally proposed to accommodate for the absence of charge-parity symmetry violation in quantum chromodynamics, i. e. the strong CP problem [4], it later became a compelling dark matter candidate [5, 6]. This theoretical sparkle triggered the first experimental searches that excluded early axion models, and which were followed by new models and new experiments [7–9]. To this day, no signal compatible with axions has been reported.

The first thing to consider when detecting a particle is its mass, and the axion one is unknown. A virtually infinite mass range can be constrained by means of models [10], astrophysics [11] and cosmology [12], suggesting a preferred window for the axion mass  $m_a$  between micro- and milli-electronvolts. Still, many theoretical efforts and experimental searches are directed towards lighter or heavier axions or axion-like particles [13]. Typically, the most sensitive experiments cover a narrow mass range, as in the case of haloscopes [14–21], while broadband techniques cover a wide mass range at the expense of a reduced sensitivity [22–24]. Among all of these are spin resonance axion searches can be based on electrons [25–27], or nuclei, which can access low frequency axions [28–31].

Dine-Fischler-Srednicki-Zhitnitsky (DFSZ) axions [32, 33] interact with fermions with pseudoscalar interaction constant  $g_p$  [34, 35] though the Lagrangian

$$\mathcal{L}_f = \frac{g_p}{2m_f} (\bar{\psi} \gamma_\mu \gamma_5 \partial^\mu a \psi), \quad (1)$$

where  $\partial^\mu a$  is the axion field quadriderivative,  $\gamma_\mu$  and  $\gamma_5$  are Dirac matrices, and  $\psi$  is the quantum field of a fermion with mass  $m_f$  and charge  $e$ . One can notice that  $\mathcal{L}_f$  is analogous to the interaction Lagrangian of quantum

## electrodynamics

$$\mathcal{L}_{\text{QED}} \supset -e(\bar{\psi} \gamma_\mu A^\mu \psi), \quad (2)$$

minus a  $\gamma_5$ . Physically, this means that the axion field derivative acts on fermionic spins as an effective magnetic field. In the non-relativistic limit Eq. (1) can be recast in terms of the fermion's spin  $s_i = \mu_f \sigma_i$ , where  $\mu_f = e/2m_f$  is the fermion magneton and  $\sigma_i$  is the Pauli vector. The remaining terms form a pseudo-magnetic axionic field

$$b_i = \frac{g_p}{2e} \partial_i a, \quad (3)$$

which oscillates at the frequency of the axion mass  $m_a$ , such that  $b_i \propto \beta_i e^{-im_a t}$ , where  $\beta_i = (\beta, 0, 0)$  is the axion speed relative to the speed of light  $c$ . If the spin  $s_i$  is in a static magnetic field  $B_i$  and in an axion effective field, both parallel to its direction, its equations of motion are Bloch equations [36]

$$\dot{s}_i / \gamma = \epsilon_{ijk} s^j (B^k + b^k), \quad (4)$$

where  $\gamma$  is the fermion gyromagnetic ratio. This equation displays a Larmor precession with an additional axion-induced spin precession [37–39], which is the core observable of the present work. Taking the non-relativistic limit of Eq. (3), and treating the axion as a classical field are justified by  $\beta_i \ll 1$  and by the large axion occupation number  $n_a = \rho_{\text{dm}}/m_a$  [27, 40], respectively. An Earth-based laboratory is immersed in the dark matter halo of the Milky Way, whose estimated density is  $\rho_{\text{dm}} = 0.4 \text{ GeV/cm}^3$ , and travels through it at a speed  $\beta \simeq 10^{-3}$ . The resulting axion effective field is

$$b_a = \frac{g_p}{2e} \beta n_a^{1/2} \simeq 3 \times 10^{-18} (m_a/1 \text{ eV}) \text{ T}. \quad (5)$$

centered at the frequency corresponding to the axion mass, and with a quality factor which is approximately  $Q_a \simeq \beta^{-2} \simeq 10^6$  [8, 40].

The detection of an axion precession can be understood in a general experimental scheme which can be realised at different energy scales—i.e. axion masses—and therefore with different physical systems and technologies, outlined in Table I. Let's first discuss the experimental scheme, outlined in Fig. 1. The spin resonance

under consideration is phase-modulated by the dark matter axion field gradient which, being dependent on  $\beta_i$ , is a directional effect. This suggests that two spin resonances with static magnetic fields oriented perpendicularly to each other can be used as the two arms of an interferometer. The east arm—(E)—is parallel to the axion field gradient and carries the dark matter signal, while the north arm—(N)—acts as a reference. In the east arm  $B_i^{(E)} = (B_0, 0, 0)$  and  $b_i = (b_a, 0, 0)$ , so Eq. (4) describes a spin resonance whose resonant frequency  $\omega_0 = \gamma B_0$  is periodically modulated by an axionic field with amplitude  $b_a$  and frequency  $\omega_a$ . The north arm has  $B_i^{(N)} = (0, B_0, 0)$ , giving the same resonance frequency and no axionic modulation. One can therefore imagine to shine the same light beam to both the resonances, and then let the outputs interfere with themselves, providing an interferometric readout of a dark matter axion signal.

This scheme is analogous to the one of gravitational wave observatories, where the Fabry-Pérot cavities are substituted by the spin resonances, as shown in Fig. 1. Although existing proposals use interferometric techniques to search for axions [41–44], the present one differs from them in both detection principle and practical realisation. As is detailed in the following, the advantages of this approach are that it leverages the considerable experimental assets of interferometry, it is broadband in the axion mass parameter space, and it can be engineered at different energy scales.

### Detection scheme

As shown in the introduction, axionic dark matter produces coherent oscillations in the frequency of a spin resonance. A suitable way to detect this effect is based on phase modulation, and is detailed in the following. A monochromatic input light on-resonance with the spin precession and with amplitude  $A_0$  is phase modulated by the oscillating resonance, yielding a signal

$$\xi(t) = A_0 e^{-i\omega_0 t} e^{-ix \sin(\omega_a t)}, \quad (6)$$

where  $x = 2\pi^2 \gamma b_a / k_0$  is the modulation index, and  $k_0$  is the spin resonance linewidth. This effect is illustrated in Fig. 2 by using a magnified effect of axions acting on a frequency  $\omega_0 / 2\pi = 5$  MHz. If the modulation index  $x$  is small,  $\xi(t)$  can be recast in terms of the first kind Bessel

	$\omega_0/2\pi$	$k_0/2\pi$	$m_a$
Spin resonance	10 MHz	100 kHz	$< 0.4$ neV
Magnon polariton	10 GHz	1 MHz	$< 40$ neV
Atomic transition	100 THz	10 GHz	$< 40$ $\mu$ eV

TABLE I. Experimental platforms to implement a fermionic axion interferometer at different energy scales.

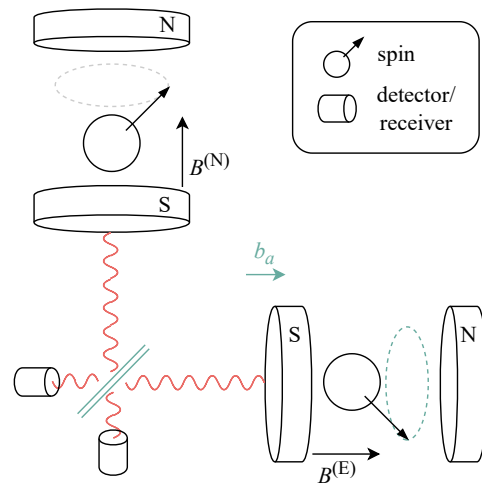


FIG. 1. Scheme illustrating the principle of a fermionic interferometer. Two perpendicular spin resonances act as arms of an interferometer, which are probed by splitted light beams. The probe signals are reported in pink while the axion field  $b_a$  is green, see text for further details.

functions

$$\xi(t) = \sum_{n=0}^{\infty} \xi_n(x) = A_0 e^{-i\omega_0 t} \sum_{n=0}^{\infty} \frac{x^n}{2^n n!} e^{in\omega_a t}. \quad (7)$$

At zero order Eq. (7) gives the monochromatic tone amplitude itself  $|\xi_0| = A_0$ , while for  $n = 1$  it yields the first sideband amplitude

$$|\xi_1| = \pi\gamma A_0 b_a / 2k_0 \quad (8)$$

which is the searched-for signal of the scheme. One can notice that the sensitivity of phase-modulation schemes to first order does not depend on the amount of material used, but rather on its coherence properties—i.e. the spin resonance linewidth  $k_0$ —making them ideal tabletop experiments [45].

Eq. (8) needs to be compared with a background to get the experimental sensitivity. While the signal calculation is general enough to accommodate for different experimental schemes, the treatment of the noise is more involved, and is discussed hereafter in some details. Assuming that the sensitivity is limited by a white noise with power spectral density  $N_0^2$ , we can calculate the minimum detectable effective axion field as

$$\begin{aligned} \sigma_a &= \frac{2k_0 N_0}{\pi\gamma A_0} \\ &= 2.27 \left( \frac{k_0}{10 \text{ kHz}} \right) \left( \frac{N_0/A_0}{10^{-5}/\sqrt{\text{Hz}}} \right) \frac{\text{pT}}{\text{Hz}^{1/2}}, \end{aligned} \quad (9)$$

where  $\gamma$  is the electron gyromagnetic ratio, and the other quantities are roughly the experimental parameters of the setup described in the next part of this work. For instance, considering an axion signal at 1 kHz and therefore

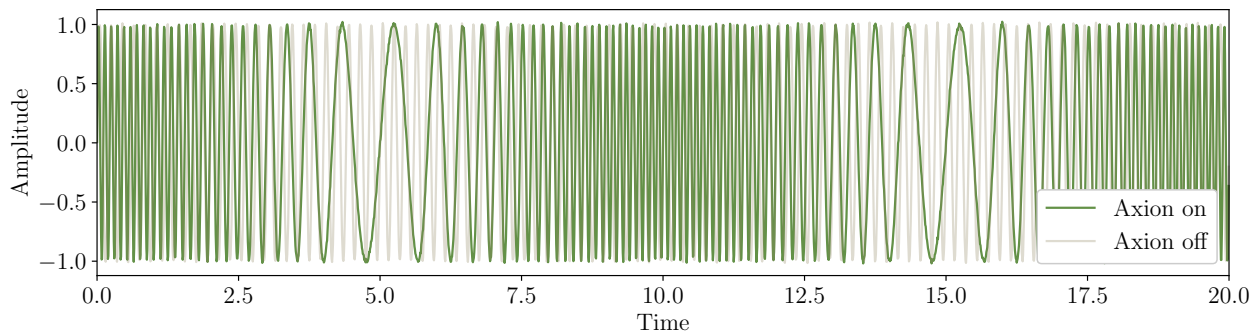


FIG. 2. Effect of the axionic modulation on a monochromatic signal interacting with a spin resonance. The axionic dark matter modulates the spin resonance frequency, thereby inducing oscillations on the phase of the monochromatic signal.

an integration time of  $10^3$  s—matching  $Q_a$ —we obtain a sensitivity of about 72 fT.

The interferometer bandwidth—the range of axion masses probed by the experiment—is in first approximation  $k_0$ , as when  $\omega_a > k_0$  the sideband  $\xi_1$  falls out of resonance, and its amplitude decreases. However, depending on the background origin, the signal-to-noise ratio could be preserved, and the experimental bandwidth could be increased depending on the measurement technique.

Let’s briefly discuss the three experimental cases of Table I, which are referred to as radiofrequency, microwave, and laser interferometer, respectively. A radiofrequency interferometer can be realised with both nuclei or electrons. The former resembles some configurations of the cosmic axion spin precession experiment [46, 47], although not searching for axion-induced oscillating dipole moments or magnetisation. However, one could use a different detection configuration of the same setup to implement the scheme described in this work. Electron spin based experiments work with low magnetic fields, which is advantageous in terms of complexity but makes it particularly sensitive to environmental fluctuations. A non-negligible advantage of radiofrequency setups is that all the interferometry can be handled digitally thanks to fast electronics, reducing the hardware requirements to a minimum. At microwave frequencies nuclear spin resonance becomes inaccessible, although some nuclei like Holmium show up to GHz precession [48, 49] thanks to a large effective  $\gamma$ . Electron spin resonances on the other hand are widely studied in this frequency range. A major problem occurring with spin resonances at high frequencies is the broadening of the resonance linewidth, often referred to as radiation damping [40], which is eliminated by embedding the sample in a resonant cavity. The resulting photon-magnon hybrid systems are applied e.g. to quantum technologies [50] and Dark Matter searches [27].

A laser axion interferometer has several intriguing features. Let us consider as an example a magnetic dipole atomic transition in the infrared range. A resonant laser

beam transmitted through the sample will experience phase modulation like the carrier signals treated beforehand, and with a quality factor of order  $10^4$  the bandwidth of the interferometer would encompass the whole QCD axion range [51]. On top of that, the experimental apparatus can benefit from all the advantages of interferometers, similarly to gravitational waves observatories. However, the effective modulation of a magnetic dipole resonance should be estimated and would probably depend on the nature of the transition itself [52].

### Experimental axion search

This section concerns the building and operation of a radiofrequency axion interferometer sensitive to the axion-electron interaction at sub-megahertz frequency [53], a scheme of the experimental setup is presented in Fig. 3.

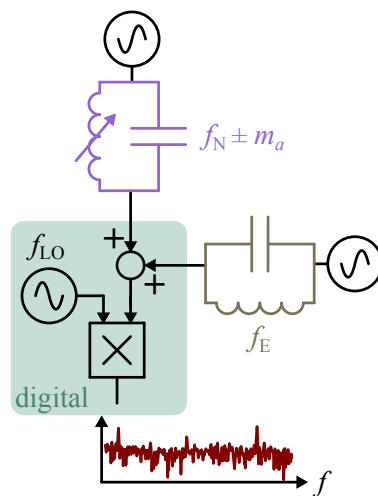


FIG. 3. Circuit scheme of the haloscope. The two resonators represent the ferrimagnetic arms of the setup, which are probed with a coherent tone each. The resulting signal is acquired with a data acquisition board and processed.

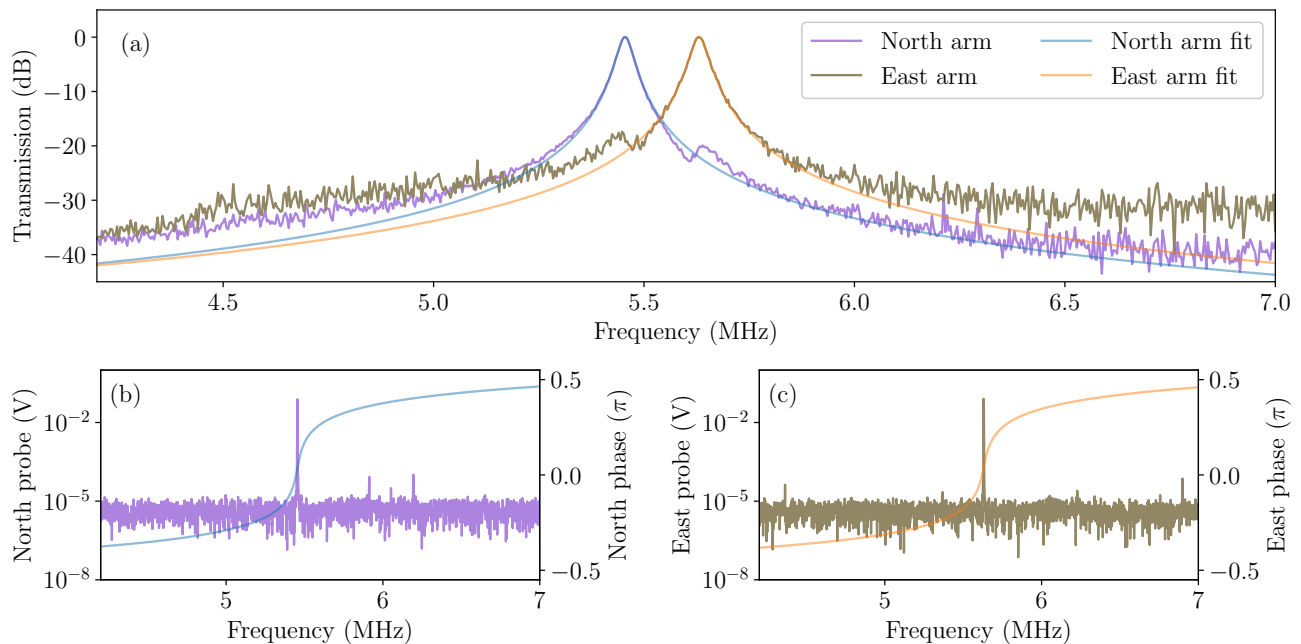


FIG. 4. Characterisation and operation of the fermionic interferometer. Panel (a) shows the transmission spectrum of the north and east resonances used to calculate the experiment properties and set the tones frequencies  $\omega_1$  and  $\omega_2$ . Panels (b) and (c) are an extract of the interferometer data while in operation, and show the probing tones superimposed to resonance phases.

The sensing material is a ferrimagnet, NiZn, shaped in two rods oriented perpendicularly. The rods are the two arms of the interferometer and are labelled north (N) and east (E) from the direction they are pointing at. Each rod is readout by coupling it to a coil, resulting in a resonance frequency of about 5 MHz, and is then connected to the electronics (for more details see the appendix).

Given the relatively low frequency of the resonances, the signal is generated and readout by a 125 MS/s analog-to-digital and digital-to-analog field-programmable-gate-array board, allowing to handle the signal processing digitally. In addition, several environmental parameters, like temperature, pressure or local magnetic field, are recorded with dedicated sensors, allowing to disentangle a possible axion signal from environmental systematics. The setup characterisation relies on the transmission measurement of the resonances, which gives the resonance frequencies of the arms, and their linewidth, as presented in Fig. 4a. The north arm has resonance frequency  $\omega_N = 5.45$  GHz and linewidth  $k_N = 19.4$  kHz, while the east arm has  $\omega_E = 5.63$  GHz and  $k_E = 21.4$  kHz, obtained by fitting the transmission measurement with Lorentzian functions.

The haloscope operation requires to send two tones on resonance with each arm to achieve the maximum phase modulation, as shown in Fig. 4b and 4c. The tones' frequency are  $\omega_N$  and  $\omega_E$ , while their amplitudes are set to  $A_N = A_E = 1.0$  V. The two analog signals are summed and down-converted according to Fig. 3, where the down-conversion frequency  $\omega_{LO} = (2\pi)f_{LO}$  needs to

be  $\omega_{LO} = (\omega_N + \omega_E)/2$ . The interferometer can suppress common phase or amplitude noise depending on the phase of the down-conversion tone [54], and given the nature of the axion signal, we opt for phase noise reduction. Eq. (9) shows that it is possible to arbitrarily improve the sensitivity by increasing  $A_0$ , i.e. using stronger tones. However, in a realistic experimental configuration  $N_0$  is directly proportional to  $A_0$ , or—in the best case scenario—dominated by quantum fluctuations. The limit of the present setup is the phase noise of the signal generators, which is about -100 dBc, and fixes  $A_0/N_0 \simeq 10^{-5}$  V/Hz<sup>1/2</sup>. As mentioned in the introduction, the virtualised axion field have  $Q_a \simeq 10^6$ , and therefore the optimal resolution bandwidth to detect it is  $RBW = \omega_a/Q_a$ . For frequencies below 200 kHz RBW is above one second, but in the present setup the resolution bandwidth is set to  $RBW = 1$  kHz, the minimum allowed by the electronics. The duty cycle of the acquisition is also limited to roughly 2%. These last two limitations are purely technical, and will be optimised in an updated version of the setup. The experiment is controlled using a dedicated characterisation, acquisition and analysis code which can be found in Ref. [53].

If one arm is oriented towards Vega [40] its resonance frequency is modulated by the axion field  $b_a$ , while the one of the remaining arm is unaltered. A single radiofrequency signal probes the on-resonance transmission of the ferrite, and indicates whether the resonance frequency shifts, while two signals, each on one arm of the interferometer, can detect relative shifts of one spin res-

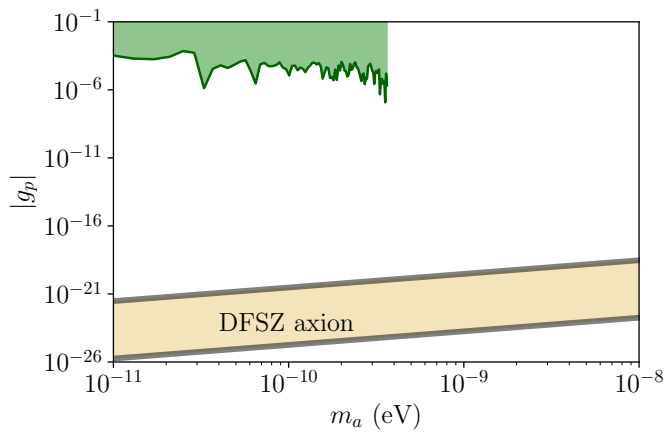


FIG. 5. Exclusion plot, and axion line [51]. Other limits (not shown) are at higher frequencies [26, 27, 55], or based on solar axion searches [56].

onance with respect to the other [54]. The measurement scheme is interferometric, and therefore resilient to systematic uncertainties. The output data (see Fig. 3) is a spectrum which contains information on whether  $\omega_N$  shifted with respect to  $\omega_E$  or viceversa, which can be used to put a limit on the presence of a dark matter wind.

An experimental run consists in the acquisition of an arbitrary number of 1 ms-long spectra which are then averaged to a single spectrum. We collect two runs of  $10^4$  s, called signal and background. The former is collected while the signal is at the maximum of its daily modulation and the latter while no signal is expected, so that by comparing them one can extract an upper limit on the axion-electron interaction. Signal and background are found to be compatible on all the measured frequencies, so the result is consistent with no axion signal. Following Eq. (5), the magnetic field limit is recast in the  $2\sigma$  (90% confidence level) upper limit on  $g_p$  reported in Fig. 5. The minimum value measured for  $|g_p|$  is  $1.2 \times 10^{-7}$  for an axion mass of about 0.36 neV.

### Perspectives and conclusions

A fermionic interferometer is a broadband dark matter axion experiment based on the modulation of spin resonances. Two light beams interact with a magnetic material whose properties depend on the local dark matter density to then interfere, eliminating systematic errors and only preserving the searched-for signal. The scheme can be realised with radiofrequency, microwave or laser light. We present the experimental implementation and operation of a radiofrequency fermionic interferometer with which we perform an axion search in the sub-neV mass range.

This preliminary setup of the interferometer is realised

in a minimal experimental scheme which is prone to improvements, and which is simple enough to be openly reproduced [53]. Short term improvements include an apparatus where the interferometry is analogic, and digitisation happens only after the down-conversion. This allows for continuous monitoring of the signal, and therefore an arbitrary resolution bandwidth and a unitary duty cycle, making it also possible to search for transient signals.

For future axion searches, in particular towards  $\mu\text{eV}$ -mass axions (see Table I), one can envision a laser interferometer probing an infrared magnetic resonance of e. g. Er:YLF or Er:YSO [57–59]. This axion experiment is particularly interesting because it leverages the analogy with gravitational waves detectors, where the magnetic resonance plays the role of the Fabry-Pérot cavity. However, a detailed studies of the atomic transition to be used is required to design and operate such experiment.

Beyond axion searches, an intriguing possibility is the use of this interferometer to detect gravitational waves effects via the gravitational Larmor [60] or gravitational precession [61, 62]. No change is necessary on the experimental setup, as it is already sensitive to any effective magnetic field modulating the spin resonance, but the analysis procedure would need to be modified in order to measure transient effects instead of persistent ones. Eventually, we mention that the magnetic field sensitivity of the setup is interesting also beyond fundamental physics, as when optimised can compete with state-of-the-art magnetometers [45, 63–66].

### Acknowledgements

The support of Amberlab, in the persons of Davide Fasoli and Manuel Pachera, is greatly acknowledged for the help and support for building the experimental apparatus. Federico Chiossi is also acknowledged for the advice on the use of atomic transitions to realise the fermionic interferometer. Eventually, the author would like to thank Gianni Carugno and Giuseppe Ruoso for the discussion on the experimental scheme.

\* ncrescini@fbk.eu

- [1] J. Ellis, *Nuclear Physics A* **827**, 187c (2009).
- [2] J. Jaeckel and A. Ringwald, *Annual Review of Nuclear and Particle Science* **60**, 405 (2010).
- [3] I. G. Irastorza, *SciPost Phys. Lect. Notes* , 45 (2022).
- [4] L. Di Luzio, M. Giannotti, E. Nardi, and L. Visinelli, *Physics Reports* **870**, 1 (2020), the landscape of QCD axion models.
- [5] F. Chadha-Day, J. Ellis, and D. J. E. Marsh, *Science Advances* **8**, eabj3618 (2022).
- [6] G. Bertone, D. Hooper, and J. Silk, *Physics Reports* **405**, 279 (2005).



- [7] I. G. Irastorza and J. Redondo, *Progress in Particle and Nuclear Physics* **102**, 89 (2018).
- [8] P. Sikivie, *Rev. Mod. Phys.* **93**, 015004 (2021).
- [9] Y. K. Semertzidis and S. Youn, *Science Advances* **8**, eabm9928 (2022).
- [10] L. Di Luzio, F. Mescia, and E. Nardi, *Phys. Rev. Lett.* **118**, 031801 (2017).
- [11] M. Giannotti, I. G. Irastorza, J. Redondo, A. Ringwald, and K. Saikawa, *Journal of Cosmology and Astroparticle Physics* **2017** (10), 010.
- [12] D. J. Marsh, *Physics Reports* **643**, 1 (2016), axion cosmology.
- [13] J. Jaeckel, G. Rybka, and L. Winslow, *Axion dark matter* (2022).
- [14] C. Bartram, T. Braine, E. Burns, R. Cervantes, N. Crisosto, N. Du, H. Korandla, G. Leum, P. Mohapatra, T. Nitta, L. J. Rosenberg, G. Rybka, J. Yang, J. Clarke, I. Siddiqi, A. Agrawal, A. V. Dixit, M. H. Awida, A. S. Chou, M. Hollister, S. Knirck, A. Sonnenschein, W. Wester, J. R. Gleason, A. T. Hipp, S. Jois, P. Sikivie, N. S. Sullivan, D. B. Tanner, E. Lentz, R. Khatiwada, G. Carosi, N. Robertson, N. Woollett, L. D. Duffy, C. Boutan, M. Jones, B. H. LaRoque, N. S. Oblath, M. S. Taubman, E. J. Daw, M. G. Perry, J. H. Buckley, C. Gaikwad, J. Hoffman, K. W. Murch, M. Goryachev, B. T. McAllister, A. Quiskamp, C. Thomson, and M. E. Tobar (ADMX Collaboration), *Phys. Rev. Lett.* **127**, 261803 (2021).
- [15] C. M. Adair, K. Altenmüller, V. Anastassopoulos, S. Arguedas Cuendis, J. Baier, K. Barth, A. Belov, D. Bozicevic, H. Bräuninger, G. Cantatore, F. Caspers, J. F. Castet, S. A. Çetin, W. Chung, H. Choi, J. Choi, T. Dafni, M. Davenport, A. Dermenev, K. Desch, B. Döbrich, H. Fischer, W. Funk, J. Galan, A. Gardikiotis, S. Gninenko, J. Golm, M. D. Hasinoff, D. H. H. Hoffmann, D. Díez Ibáñez, I. G. Irastorza, K. Jakovčić, J. Kaminski, M. Karuza, C. Krieger, Ç. Kutlu, B. Lakić, J. M. Laurent, J. Lee, S. Lee, G. Luzón, C. Malbrunot, C. Margalejo, M. Maroudas, L. Miceli, H. Mirallas, L. Obis, A. Özbey, K. Özbozduman, M. J. Pivovarov, M. Rosu, J. Ruz, E. Ruiz-Chóliz, S. Schmidt, M. Schumann, Y. K. Semertzidis, S. K. Solanki, L. Stewart, I. Tsagris, T. Vafeiadis, J. K. Vogel, M. Vretenar, S. Youn, and K. Zioutas, *Nature Communications* **13**, 6180 (2022).
- [16] A. K. Yi, S. Ahn, i. m. c. b. u. Kutlu, J. Kim, B. R. Ko, B. I. Ivanov, H. Byun, A. F. van Loo, S. Park, J. Jeong, O. Kwon, Y. Nakamura, S. V. Uchaikin, J. Choi, S. Lee, M. Lee, Y. C. Shin, J. Kim, D. Lee, D. Ahn, S. Bae, J. Lee, Y. Kim, V. Gkika, K. W. Lee, S. Oh, T. Seong, D. Kim, W. Chung, A. Matlashov, S. Youn, and Y. K. Semertzidis, *Phys. Rev. Lett.* **130**, 071002 (2023).
- [17] D. Alesini, D. Babusci, C. Braggio, G. Carugno, N. Crescini, D. D'Agostino, A. D'Elia, D. Di Gioacchino, R. Di Vora, P. Falferi, U. Gambardella, C. Gatti, G. Iannone, C. Ligi, A. Lombardi, G. Maccarrone, A. Ortolan, R. Pengo, A. Rettaroli, G. Ruoso, L. Taffarello, and S. Tocci, *Phys. Rev. D* **106**, 052007 (2022).
- [18] B. M. Brubaker, L. Zhong, Y. V. Gurevich, S. B. Cahn, S. K. Lamoreaux, M. Simanovskaia, J. R. Root, S. M. Lewis, S. Al Kenany, K. M. Backes, I. Urdinaran, N. M. Rapidis, T. M. Shokair, K. A. van Bibber, D. A. Palken, M. Malnou, W. F. Kindel, M. A. Anil, K. W. Lehnert, and G. Carosi, *Phys. Rev. Lett.* **118**, 061302 (2017).
- [19] B. T. McAllister, G. Flower, E. N. Ivanov, M. Goryachev, J. Bourhill, and M. E. Tobar, *Physics of the Dark Universe* **18**, 67 (2017).
- [20] A. J. Millar, S. M. Anlage, R. Balafendiev, P. Belov, K. van Bibber, J. Conrad, M. Demarteau, A. Droster, K. Dunne, A. G. Rosso, J. E. Gudmundsson, H. Jackson, G. Kaur, T. Klaesson, N. Kowitt, M. Lawson, A. Leder, A. Miyazaki, S. Morampudi, H. V. Peiris, H. S. Røising, G. Singh, D. Sun, J. H. Thomas, F. Wilczek, S. Withington, M. Wooten, J. Dilling, M. Febraro, S. Knirck, and C. Marvinney (Endorsers), *Phys. Rev. D* **107**, 055013 (2023).
- [21] T. Grenet, R. Ballou, Q. Basto, K. Martineau, P. Perrier, P. Pignat, J. Quevillon, N. Roch, and C. Smith, *The grenoble axion haloscope platform (grahal): development plan and first results* (2021), arXiv:2110.14406 [hep-ex].
- [22] C. P. Salemi, J. W. Foster, J. L. Ouellet, A. Gavin, K. M. W. Pappas, S. Cheng, K. A. Richardson, R. Henning, Y. Kahn, R. Nguyen, N. L. Rodd, B. R. Safdi, and L. Winslow, *Phys. Rev. Lett.* **127**, 081801 (2021).
- [23] A. V. Gramolin, D. Aybas, D. Johnson, J. Adam, and A. O. Sushkov, *Nature Physics* **17**, 79 (2021).
- [24] V. Anastassopoulos, S. Aune, K. Barth, A. Belov, H. Bräuninger, G. Cantatore, J. M. Carmona, J. F. Castet, S. A. Cetin, F. Christensen, J. I. Collar, T. Dafni, M. Davenport, T. A. Decker, A. Dermenev, K. Desch, C. Eleftheriadis, G. Fanourakis, E. Ferrer-Ribas, H. Fischer, J. A. García, A. Gardikiotis, J. G. Garza, E. N. Gazis, T. Gerasis, I. Giomataris, S. Gninenko, C. J. Hailey, M. D. Hasinoff, D. H. H. Hoffmann, F. J. Iguaz, I. G. Irastorza, A. Jakobsen, J. Jacoby, K. Jakovčić, J. Kaminski, M. Karuza, N. Kralj, M. Krčmar, S. Kostoglou, C. Krieger, B. Lakić, J. M. Laurent, A. Liolios, A. Ljubičić, G. Luzón, M. Maroudas, L. Miceli, S. Neff, I. Ortega, T. Papaevangelou, K. Paraschou, M. J. Pivovarov, G. Raffelt, M. Rosu, J. Ruz, E. R. Chóliz, I. Savvidis, S. Schmidt, Y. K. Semertzidis, S. K. Solanki, L. Stewart, T. Vafeiadis, J. K. Vogel, S. C. Yildiz, K. Zioutas, and C. A. S. T. Collaboration, *Nature Physics* **13**, 584 (2017).
- [25] N. Crescini, D. Alesini, C. Braggio, G. Carugno, D. Di Gioacchino, C. S. Gallo, U. Gambardella, C. Gatti, G. Iannone, G. Lamanna, C. Ligi, A. Lombardi, A. Ortolan, S. Pagano, R. Pengo, G. Ruoso, C. C. Speake, and L. Taffarello, *The European Physical Journal C* **78**, 703 (2018).
- [26] G. Flower, J. Bourhill, M. Goryachev, and M. E. Tobar, *Physics of the Dark Universe* **25**, 100306 (2019).
- [27] N. Crescini, D. Alesini, C. Braggio, G. Carugno, D. D'Agostino, D. Di Gioacchino, P. Falferi, U. Gambardella, C. Gatti, G. Iannone, C. Ligi, A. Lombardi, A. Ortolan, R. Pengo, G. Ruoso, and L. Taffarello (QUAX Collaboration), *Phys. Rev. Lett.* **124**, 171801 (2020).
- [28] T. Wu, J. W. Blanchard, G. P. Centers, N. L. Figueroa, A. Garcon, P. W. Graham, D. F. J. Kimball, S. Rajendran, Y. V. Stadnik, A. O. Sushkov, A. Wickenbrock, and D. Budker, *Phys. Rev. Lett.* **122**, 191302 (2019).
- [29] A. Garcon, J. W. Blanchard, G. P. Centers, N. L. Figueroa, P. W. Graham, D. F. J. Kimball, S. Rajendran, A. O. Sushkov, Y. V. Stadnik, A. Wickenbrock, T. Wu, and D. Budker, *Science Advances* **5**, eaax4539 (2019), <https://www.science.org/doi/pdf/10.1126/sciadv.aax4539>.

- [30] D. F. Jackson Kimball, S. Afach, D. Aybas, J. W. Blanchard, D. Budker, G. Centers, M. Engler, N. L. Figueroa, A. Garcon, P. W. Graham, H. Luo, S. Rajendran, M. G. Sendra, A. O. Sushkov, T. Wang, A. Wickenbrock, A. Wilzewski, and T. Wu, in *Microwave Cavities and Detectors for Axion Research*, edited by G. Carosi and G. Rybka (Springer International Publishing, Cham, 2020) pp. 105–121.
- [31] J. W. Blanchard, A. O. Sushkov, and A. Wickenbrock, Magnetic resonance searches, in *The Search for Ultralight Bosonic Dark Matter*, edited by D. F. Jackson Kimball and K. van Bibber (Springer International Publishing, Cham, 2023) pp. 173–200.
- [32] M. Dine, W. Fischler, and M. Srednicki, *Physics Letters B* **104**, 199 (1981).
- [33] A. R. Zhitnitsky, *Sov. J. Nucl. Phys.* **31**, 529 (1980).
- [34] R. Barbieri, M. Cerdonio, G. Fiorentini, and S. Vitale, *Physics Letters B* **226**, 357 (1989).
- [35] J. Sun and X.-G. He, *Physics Letters B* **811**, 135881 (2020).
- [36] N. Ashcroft and N. Mermin, *Solid State Physics* (Cengage Learning, 2011).
- [37] J. E. Moody and F. Wilczek, *Phys. Rev. D* **30**, 130 (1984).
- [38] A. B. Balakin and V. A. Popov, *Phys. Rev. D* **92**, 105025 (2015).
- [39] Z. Wang and L. Shao, *Phys. Rev. D* **103**, 116021 (2021).
- [40] R. Barbieri, C. Braggio, G. Carugno, C. Gallo, A. Lombardi, A. Ortolan, R. Pengo, G. Ruoso, and C. Speake, *Physics of the Dark Universe* **15**, 135 (2017).
- [41] W. DeRocco and A. Hook, *Phys. Rev. D* **98**, 035021 (2018).
- [42] I. Obata, T. Fujita, and Y. Michimura, *Phys. Rev. Lett.* **121**, 161301 (2018).
- [43] H. Liu, B. D. Elwood, M. Evans, and J. Thaler, *Phys. Rev. D* **100**, 023548 (2019).
- [44] D. Martynov and H. Miao, *Phys. Rev. D* **101**, 095034 (2020).
- [45] N. Crescini, G. Carugno, and G. Ruoso, *Phys. Rev. Appl.* **16**, 034036 (2021).
- [46] P. W. Graham and S. Rajendran, *Phys. Rev. D* **88**, 035023 (2013).
- [47] D. Budker, P. W. Graham, M. Ledbetter, S. Rajendran, and A. O. Sushkov, *Phys. Rev. X* **4**, 021030 (2014).
- [48] D. S. P. Bunbury, C. Carboni, and M. A. H. McCausland, *Journal of Physics C: Solid State Physics* **18**, L1151 (1985).
- [49] D. S. P. Bunbury, C. Carboni, and M. A. H. McCausland, *Journal of Physics: Condensed Matter* **1**, 1309 (1989).
- [50] Y. Tabuchi, S. Ishino, T. Ishikawa, R. Yamazaki, K. Usami, and Y. Nakamura, *Phys. Rev. Lett.* **113**, 083603 (2014).
- [51] C. O'Hare, cajohare/axionlimits: Axionlimits, <https://cajohare.github.io/AxionLimits/> (2020).
- [52] The effective amplitude modulation and the noise estimation are not trivial, therefore a thorough discussion of this setup will be carried out in a forthcoming work.
- [53] N. Crescini, Open-haloscope repository, <https://github.com/ncr292/Open-Haloscope> (2023).
- [54] N. Crescini, E. Kelly, G. Salis, and A. Fuhrer, *Phys. Rev. Appl.* **20**, 044072 (2023).
- [55] Crescini, N., Alesini, D., Braggio, C., Carugno, G., Di Gioacchino, D., Gallo, C. S., Gambardella, U., Gatti, C., Iannone, G., Lamanna, G., Ligi, C., Lombardi, A., Ortolan, A., Pagano, S., Pengo, R., Ruoso, G., Speake, C. C., and Taffarello, L., *Eur. Phys. J. C* **78**, 703 (2018).
- [56] Y. M. Gavriluk, A. N. Gangapshev, A. V. Derbin, I. S. Drachnev, V. V. Kazalov, V. V. Kuzminov, M. S. Mikulich, V. N. Muratova, D. A. Tekueva, E. V. Unzhakov, and S. P. Yakimenko, *JETP Letters* **116**, 11 (2022).
- [57] R. M. Macfarlane, *Journal of Luminescence* **100**, 1 (2002).
- [58] N. Kukharchyk, D. Sholokhov, O. Morozov, S. L. Korablava, A. A. Kalachev, and P. A. Bushev, *New Journal of Physics* **20**, 023044 (2018).
- [59] T. Böttger, C. W. Thiel, R. L. Cone, and Y. Sun, *Phys. Rev. B* **79**, 115104 (2009).
- [60] B. Mashhoon, *Physics letters.* **173** (1993-2).
- [61] D. Bini, A. Geralico, and A. Ortolan, *Phys. Rev. D* **95**, 104044 (2017).
- [62] M. L. Ruggiero and A. Ortolan, *Phys. Rev. D* **102**, 101501 (2020).
- [63] J. F. Barry, R. A. Irion, M. H. Steinecker, D. K. Freeman, J. J. Kedziora, R. G. Wilcox, and D. A. Braje, *Phys. Rev. Appl.* **19**, 044044 (2023).
- [64] K. Wei, T. Zhao, X. Fang, Z. Xu, C. Liu, Q. Cao, A. Wickenbrock, Y. Hu, W. Ji, J. Fang, and D. Budker, *Phys. Rev. Lett.* **130**, 063201 (2023).
- [65] J. Clarke and A. I. Braginski, *The SQUID Handbook Fundamentals and Technology of SQUIDS and SQUID Systems*, Vol. 1 (Wiley-VCH, Weinheim, 2006).
- [66] V. Lucivero, W. Lee, M. Limes, E. Foley, T. Kornack, and M. Romalis, *Phys. Rev. Appl.* **18**, L021001 (2022).

### Appendix: open source project

The simple hardware requirements of the experiment make it interesting for open source projects to be carried out in schools, universities or by amateurs. The described experimental setup is inexpensive and all of the necessary code, from drivers to analysis routines, is publicly available [53]. A circuit-board scheme of the experiment is sketched in Fig. 6.

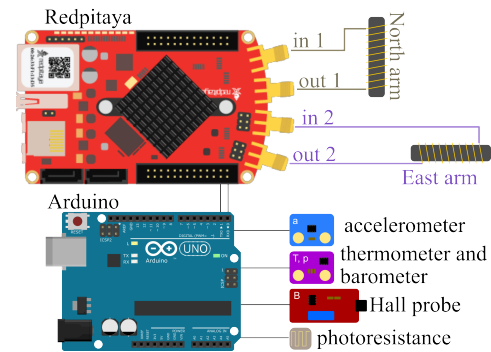


FIG. 6. Circuit board scheme of the haloscope.